

## Formation of monodisperse bubbles in a microfluidic flow-focusing device

Piotr Garstecki, Irina Gitlin, Willow DiLuzio, and George M. Whitesides<sup>a)</sup>

*Department of Chemistry and Chemical Biology, Harvard University, Cambridge, Massachusetts*

Eugenia Kumacheva

*Department of Chemistry, University of Toronto, Toronto, Ontario, Canada*

Howard A. Stone

*Division of Engineering and Applied Sciences, Harvard University, Cambridge, Massachusetts*

(Received 29 March 2004; accepted 21 July 2004)

This letter describes a method for generating monodisperse gaseous bubbles in a microfluidic flow-focusing device. The bubbles can be obtained in a range of diameters from 10 to 1000  $\mu\text{m}$ . The volume  $V_b$  of the bubbles scales with the flow rate  $q$  and the viscosity  $\mu$  of the liquid, and the pressure  $p$  of the gas stream as  $V_b \propto p/q\mu$ . This method allows simultaneous, independent control of the size of the individual bubbles and volume fraction of the dispersed phase. Under appropriate conditions, bubbles self-assemble into highly ordered, flowing lattices. Structures of these lattices can be adjusted dynamically by changing the flow parameters. © 2004 American Institute of Physics. [DOI: 10.1063/1.1796526]

This letter describes a microfluidic method for a direct on-chip generation of monodisperse gaseous bubbles with simultaneous and independent control over the size of the bubbles and volume fraction of the dispersed phase. Microfluidic devices are becoming important for applications in on-chip separation,<sup>1-3</sup> high-throughput screening,<sup>4</sup> protein crystallization,<sup>5,6</sup> and kinetic analysis.<sup>7,8</sup> These devices require the control of small volumes of fluids, and the understanding of multiphase flows. Liquid-liquid dispersions have been generated via a number of methods, including both geometry-dominated breakup<sup>9,10</sup> and flow-dominated rupturing.<sup>11-16</sup> Less work has dealt with gas-liquid dispersions. For example, Ganan-Calvo *et al.*<sup>17</sup> described the formation of monodisperse gas bubbles in capillaries. They reported a high Reynolds number scaling that is independent of the fluid viscosity. Here, we describe a flow-focusing device incorporated directly into a microfluidic chip and capable of delivering bubbles at frequencies exceeding  $10^5$  bubbles per second. In a wide range of flow parameters the polydispersity index  $\sigma$ , defined as the standard deviation of the volume of the bubble divided by the mean volume, is  $<2\%$ . In our system viscous effects are important. It operates at low-to-moderate  $Re$ <sup>18</sup> and is therefore compatible with conditions of microfluidic devices.

We fabricated the flow-focusing devices<sup>12</sup> (Fig. 1) using soft lithography.<sup>19,20</sup> We assembled the devices by placing Polydimethylsiloxane (PDMS) stamps in contact with glass cover slides. We filled the channels with water immediately after sealing to ensure the hydrophilic character of the walls of the microchannels.<sup>20</sup> The contact angle of aqueous solutions used in our study on freshly oxidized PDMS was less than  $30^\circ$ . We supplied nitrogen through the gas inlet channel from a pressurized tank via a pressure-reduction valve. The liquid was pumped using a digitally controlled syringe pump (Harvard Apparatus PhD2000). We used three different liquids: pure water (viscosity  $\mu=0.92$  mPa) and two aqueous solutions of glycerol, 52% (w/w) ( $\mu=6.1$  mPa) and 62% (w/w) ( $\mu=10.84$  mPa).<sup>21</sup> Apart from one set of experiments, all of the

liquids also contained 2% (w/w) Tween-20 surfactant. After changing any of the flow parameters, we allowed at least 60 s of equilibration time. We used a Nikon camera to capture still images and Phantom high-speed cameras to capture movies (capturing frame rates up to 160 kHz). We used homemade image analysis software to measure the areas of the interface between the bubbles and the top wall of the channel. We calculated the frequency of breakup by inspecting the movies and counting bubbles formed in a given interval.

The liquid and gas phases form an interface upstream of the orifice. The pressure drop along the longitudinal axis of the device forces the tip of the gas stream into the orifice. The tip proceeds through the orifice and fills a disk-like gas cavity downstream of the orifice (see Fig. 1). The growing bubble displaces and pushes away the liquid in the outlet channel. In the orifice, because of the hydrophilic character of the channel walls, the gaseous thread is surrounded by continuous liquid film. Due to the high surface energy of this configuration, the thread is not dynamically stable and it breaks to release a bubble into the outlet channel. Over a wide range of flow parameters, the system establishes a simply periodic ("period-1") state. In each period, a single bubble is formed, and the tip of the gas stream comes back to its initial position upstream of the orifice. For a fixed gas

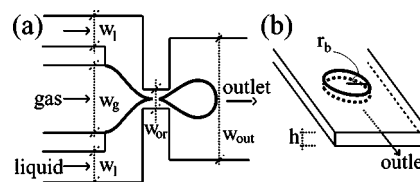


FIG. 1. (a) The microfluidic flow-focusing device (top view). The cross sections of the channels are rectangular. The widths of the inlet channels were set to  $w_l=250$   $\mu\text{m}$  and  $w_g=200$   $\mu\text{m}$  for the liquid and gas, respectively. We used several widths of the orifice  $w_{or} \in \{30, 60, 90, 120$   $\mu\text{m}\}$  and of outlet channel  $w_{out} \in \{250, 500, 750, 1000$   $\mu\text{m}\}$ . The actual dimensions did not differ from the designed ones by more than 3  $\mu\text{m}$ . All devices had the same height  $h=28$   $\mu\text{m}$ . (b) Illustration of a bubble in the outlet channel. Bubbles are squeezed between the top and bottom wall, and have a disc-like geometry. We approximate the volume of the bubble is  $V_b = \pi r_b^2 h$ , where  $r_b$  is the radius of the bubble-wall interface.

<sup>a)</sup>Electronic mail: gwhitesides@gmwhgroup.harvard.edu

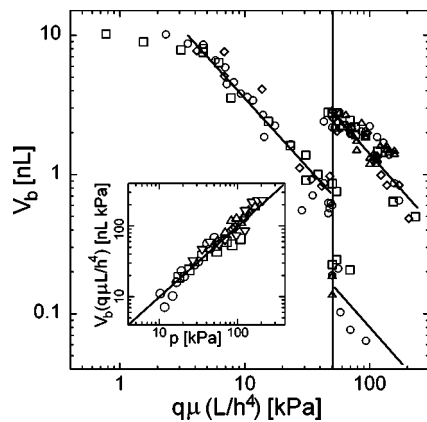


FIG. 2. Volume of the bubbles plotted against the product of the flow rate  $q$  and viscosity  $\mu$  of the liquid, and scaled to the units of pressure by multiplying by  $L/h^4$ . All experiments were performed with  $p=27.6$  kPa and with following geometrical parameters:  $w_{or}=30$   $\mu\text{m}$ ,  $w_{out}=750$   $\mu\text{m}$ , and  $L=30$  mm. Symbols correspond to different viscosities and interfacial tensions ( $\circ$ )  $\mu=0.92$  mPa,  $\gamma=37.0$  mN/m; ( $\Delta$ )  $\mu=0.92$  mPa,  $\gamma=72$  mN/m; ( $\square$ )  $\mu=6.1$  mPa,  $\gamma=31.6$  mN/m; and ( $\diamond$ )  $\mu=10.84$  mPa,  $\gamma=33.1$  mN/m. The solid lines give the slope of a relation  $(q\mu)^{-1}$ . The vertical line marks the transition from the period 1 to period 2. The inset shows scaling of the bubble size with pressure. Five series of data are shown for ( $\mu=0.92$  mPa,  $\gamma=37$  mN/m) and five different flow rates: ( $\circ$ ) 0.278, ( $\square$ ) 0.556, ( $\diamond$ ) 1.39, ( $\Delta$ ) 2.78, and ( $\nabla$ ) 5.66  $\mu\text{L/s}$ . We multiplied  $V_b$  by  $q\mu L/h^4$  to leave only the dependence on pressure. The solid line gives the slope of a linear relation between  $V_b$  and  $p$ .

pressure, an increase in the rate of flow of the liquid results in a decrease of the bubble size. For a given geometry of the channel and gas pressure, there is a critical liquid flow rate above which the system transitions into a “period-2” behavior, characterized by the formation of two bubbles of different sizes in each cycle. After the first bubble is released, the tip of the gas stream stays in the orifice and continues to elongate, until it breaks again and releases a second bubble. After the second breakup, the tip retracts upstream from the orifice and the sequence is repeated.

Within the period-1 regime, we have produced bubbles having radii between 5 and 500  $\mu\text{m}$  by varying  $q$  and  $p$ . We have measured frequencies of formation above  $f > 100$  kHz. In the period-1 regime, the bubbles are almost ideally monodisperse. The polydispersity index  $\sigma$  falls well below 5%. The actual values established via the image recognition software range from 1% to 2% and lie within the measurement error. The uniformity of the bubbles decreases substantially at the transition between period-1 and period-2 regimes, up to  $\sigma=15\%$ . In the period-2 regime,  $\sigma$  is again well below 5%, when calculated for large and small bubbles separately.

In order to establish the scaling of the size of the bubbles, we varied the gas pressure  $p$ , the flow rate  $q$ , and the viscosity  $\mu$  of the liquid. We also examined formation of the bubbles in the absence of surfactant. We observed that: (i) the volumes of the bubbles  $V_b$  collapse on a single master curve when plotted as a function of the product of  $q$  and  $\mu$  (see Fig. 2); (ii)  $V_b$  increases with an increase of  $p$ ; and (iii) a twofold increase of the surface tension<sup>22</sup> did not induce any substantial change in the volume of the bubbles.

The observation that  $V_b$  is inversely proportional to the product of viscosity and flow rate ( $V_b \propto 1/\mu q$ ) suggests the capillary number  $\text{Ca} = u\mu/\gamma$ , where  $u \propto q$  is the average velocity of the liquid, as the nondimensional parameter governing the breakup dynamics. To check this hypothesis we changed the surface tension from  $\gamma=37$  mN/m [2% (w/w)

Tween-20] to  $\gamma=72$  mN/m (no surfactant).<sup>22</sup> In the absence of surfactant, the bubbles coalesce immediately as they touch each other in the outlet channel. We were able to determine their size by inspection of the movies recorded with the high-speed cameras. Surprisingly, the twofold increase in  $\gamma$  did not influence the volume of the bubbles substantially. This result excludes the capillary number as the relevant parameter, and suggests a breakup mechanism that is not simply a competition between the shear stress and surface tension. Finally, for a fixed  $q$ , the relation between the volume of the bubble and the gas pressure is linear (inset in Fig. 2).

The volume of the bubble  $V_b$  is equal to the rate  $q_{gas}$  at which the bubble expands in the outlet channel times the interval  $\tau$  between the entrance of the gaseous thread into the orifice and the pinch off. The flow in the outlet channel is subject to viscous resistance, and the rate of expansion  $q_{gas}$  of the bubble can be estimated by the Poiseuille equation of viscous resistance  $R$  to flow  $R \cong \mu L/h^4$ , where the height of the channel  $h$  is the relevant cross-sectional length scale and  $L$  is the length of the outlet channel. Thus,  $q_{gas} = p/R \propto p/\mu$ . From a detailed study of the breakup mechanism,<sup>23</sup> in which we carefully inspect the evolution of the shape of the gaseous thread during breakup, we know that the velocity of collapse—the change of the minimal width of the thread in time—is limited by the flow rate  $q$  of the continuous fluid, yielding  $\tau \propto 1/q$ . Combining  $q_{gas}$  and  $\tau$  together gives  $V_b \propto p/q\mu$ , as observed experimentally.

The volume of the bubble depends only on the ratio of the pressure  $p$  and flow-rate  $q$ . By keeping this ratio constant, we can control the volume fraction of the dispersed phase independently of the size of the bubbles. We define the volume fraction  $\phi_{or}$  as the ratio of the average flow rates at which the two fluids exit the orifice:  $\phi_{or} = fV_b/(fV_b + q)$ , where  $f$  is the frequency of breakup and  $V_b$  is the volume of a single bubble. Interestingly, the volume fraction  $\phi_{ch}$  of the bubbles in the outlet channel—the ratio of the volume occupied by the bubbles to the volume of the outlet channel—is different ( $\phi_{ch} \neq \phi_{or}$ ). Due to the viscous dissipation in thin films between the bubbles and the walls of the channel, the bubbles move slower than the liquid.<sup>24,25</sup> The ratio of the flow rates of gas and liquid is preserved, but the volume fractions are not. Knowing  $\phi_{ch}$  and  $f$  allows a calculation of the velocity of the bubbles. Such estimates should be interesting for studies concerning the flow of bubbles, droplets, and plugs in narrow channels. Figure 3 shows the frequency of breakup, the radius of the bubbles, and the volume fractions  $\phi_{or}$  and  $\phi_{ch}$  as functions of the liquid flow rate. For each measurement the gas pressure was adjusted so as to keep the  $p/q$  ratio constant.

In the outlet channel, the bubbles interact both by elastic shape-restoring forces when colliding with each other, and indirectly, by affecting the liquid flow field. Even when  $\phi_{ch}$  is much smaller than the limit for packing of circles in two dimensions (0.91), bubbles organize into highly ordered, flowing lattices. We propose that the reason for this behavior lies in the elastic nature of the polymer comprising the microfluidic device. The pressure difference between the inside and outside of the channel causes it to be slightly bulged upwards with a maximum height at its center. Bubbles gather in this location to minimize their interfacial area by adopting more spherical shapes. The insets in Fig. 3(a) show examples of such lattices. When  $\phi_{ch} \approx 0.9$ , bubbles pack into ordered lattices that occupy the whole cross section of the channel.

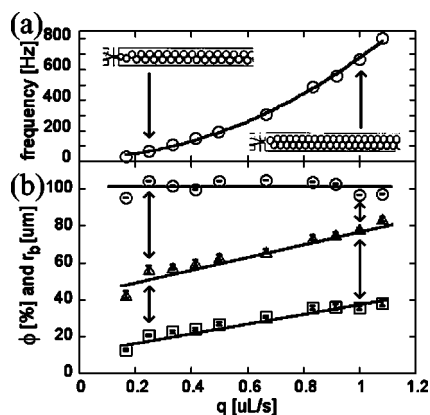


FIG. 3. (a) Frequency  $f$  of breakup plotted against the flow rate  $q$  of the liquid. The pressure to flow-rate ratio was kept constant for all the data points. The solid line gives a fit  $f \propto pq$ . The dimensions of the channel are  $w_{or}=60 \mu\text{m}$ ,  $w_{out}=500 \mu\text{m}$ . (b) (○) The radius of the bubbles formed in the same experiment, (Δ) the volume fraction  $\phi_{ch}$  of bubbles in the channel, and (□) the volume fraction at which bubbles were formed  $\phi_{or}$ . The arrows mark the data points for which snapshots of the system are shown as insets to plot (a).

The ability to control size and volume fraction independently gives access to a variety of regular structures (Fig. 4). Above the volume fraction of a two-dimensional (2D) close-packed lattice, bubbles are forced to distort their circular shapes, and the flowing lattice becomes a dynamically assembled foam.

We have demonstrated a microfluidic bubble generator that operates at low  $Re$  numbers. A device containing a single orifice produces up to several hundred thousand bubbles per second with the polydispersity index as low as 1%-2%. Our system provides simultaneous, independent control of both the size and volume fraction of the dispersion. In a wide range of flow parameters, bubbles self-assemble into highly ordered, dynamically adjustable, flowing lattices.

Our observations on scaling of the size of the bubbles suggest that the dynamics of breakup in a flow-focusing device cannot be explained by a competition between the shear stress and interfacial tension. We can speculate that the period-doubling phenomenon is a result of the balance between the Laplace pressure pulling the tip upstream of the orifice, where it has a lower curvature, and of the distribution

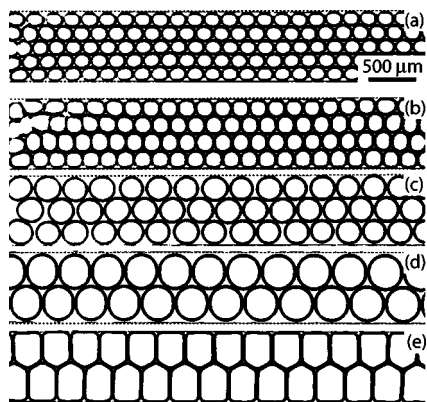


FIG. 4. Examples of the flowing lattices formed by the bubbles in the outlet channel. The outlet channel width is  $w_{out}=750 \mu\text{m}$ , the orifice width  $w_{or}=30 \mu\text{m}$ , and the pressure is set to a constant value of  $p=27.6 \text{ kPa}$ . The liquid flow rates were as follows: (a) 0.2, (b) 0.14, (c) 0.0278, (d) 0.0056, and (e) 0.0028  $\mu\text{L/s}$ . Color stills have been converted to black and white images.

of pressure in the continuous liquid. Since we also observe the transition from period-1 to period-2 bubbling in a system without surfactant, it cannot be attributed to dynamical surface-tension effects.

We believe that the gas-liquid dispersions in microfluidic systems will find applications ranging from pumping and mixing<sup>26</sup> to generating bubbles for ultrasound contrast agents.<sup>27</sup> The flowing lattices of bubbles might find applications in controlled construction of porous materials or in optics as adjustable diffraction gratings.

We thank the Harvard DEAS Microfluidics Discussion Group for helpful conversations and the Harvard MRSEC for the use of high-speed cameras. P.G. acknowledges a fellowship from the Foundation for Polish Science. I.G. thanks the NSF for a pre-doctoral fellowship. E.K. thanks CRC funding. H.A.S. thanks Unilever for support. This work was supported by the U.S. Department of Energy (DE-FG02-00ER45852).

<sup>1</sup>A. Y. Fu, C. Spence, A. Scherer, F. H. Arnold, and S. R. Quake, *Nat. Biotechnol.* **17**, 1109 (1999).

<sup>2</sup>J. D. Ramsey, S. C. Jacobson, C. T. Culbertson, and J. M. Ramsey, *Anal. Chem.* **75**, 3758 (2003).

<sup>3</sup>X. Chen, H. Wu, C. Mao, and G. M. Whitesides, *Anal. Chem.* **74**, 1772 (2002).

<sup>4</sup>J. Sinclair, J. Pihl, J. Olofsson, M. Karlsson, K. Jardemark, D. T. Chiu, and O. Orwar, *Anal. Chem.* **74**, 6133 (2002).

<sup>5</sup>C. L. Hansen, E. Skordalakes, J. M. Berger, and S. R. Quake, *Proc. Natl. Acad. Sci. U.S.A.* **99**, 16531 (2002).

<sup>6</sup>B. Zheng, L. S. Roach, and R. F. Ismagilov, *J. Am. Chem. Soc.* **125**, 11170 (2003).

<sup>7</sup>H. Song and R. F. Ismagilov, *J. Am. Chem. Soc.* **125**, 14613 (2003).

<sup>8</sup>G. H. Seong, J. Heo, and R. M. Crooks, *Anal. Chem.* **75**, 3161 (2003).

<sup>9</sup>D. R. Link, S. L. Anna, D. A. Weitz, and H. A. Stone, *Phys. Rev. Lett.* **92**, 054503/1 (2004).

<sup>10</sup>S. Sugiura, M. Nakajima, S. Iwamoto, and M. Seki, *Langmuir* **17**, 5562 (2001).

<sup>11</sup>T. Thorsen, R. W. Roberts, F. H. Arnold, and S. R. Quake, *Phys. Rev. Lett.* **86**, 4163 (2001).

<sup>12</sup>S. L. Anna, N. Bontoux, and H. A. Stone, *Appl. Phys. Lett.* **82**, 364 (2003).

<sup>13</sup>D. Rudhardt, A. Fernandez-Nieves, D. R. Link, and D. A. Weitz, *Appl. Phys. Lett.* **82**, 2610 (2003).

<sup>14</sup>R. Dreyfus, P. Tabeling, and H. Willaime, *Phys. Rev. Lett.* **90**, 144505/1 (2003).

<sup>15</sup>H. A. Stone, A. D. Stroock, and A. Ajdari, *Annu. Rev. Fluid Mech.* **36**, 381 (2004).

<sup>16</sup>O. A. Basaran, *AIChE J.* **48**, 1842 (2002).

<sup>17</sup>A. M. Ganan-Calvo and J. M. Gordillo, *Phys. Rev. Lett.* **87**, 274501 (2001).

<sup>18</sup>Reynolds number  $Re$  number is defined as  $\rho uL/\mu$ , where  $\rho$  is the density of the fluid,  $u$  is the velocity,  $\mu$  is viscosity, and  $L$  is the relevant dimension of the channel. In the range of flow parameters tested, the  $Re$  number for the flow of the continuous fluid in the orifice was  $Re=0.01-10$  and in the outlet channel  $Re \ll 1$ .

<sup>19</sup>J. C. McDonald, D. C. Duffy, J. R. Anderson, D. T. Chiu, H. Wu, and G. M. Whitesides, *Electrophoresis* **21**, 27 (2000).

<sup>20</sup>D. C. Duffy, J. C. McDonald, O. J. A. Schueller, and G. M. Whitesides, *Anal. Chem.* **70**, 4974 (1998).

<sup>21</sup>Data from Dow-Corning tables of viscosity of water-glycerol mixtures, calculated for 24°C.

<sup>22</sup>We have measured the interfacial tensions between our solutions and air,  $\gamma=37 \text{ mN/m}$  [2% (w/w) Tween-20],  $\gamma=31.6 \text{ mN/m}$  [2% (w/w) Tween-20, 52% (w/w) glycerol], and  $\gamma=33.1 \text{ mN/m}$  [2% (w/w) Tween-20, 62% (w/w) glycerol]. For a clean water-nitrogen interface we have assumed the value for water-air interface  $\gamma=72 \text{ mN/m}$ .

<sup>23</sup>P. Garstecki, H. A. Stone, and G. M. Whitesides (submitted).

<sup>24</sup>H. Wong, C. J. Radke, and S. Morris, *J. Fluid Mech.* **292**, 71 (1995).

<sup>25</sup>H. Wong, C. J. Radke, and S. Morris, *J. Fluid Mech.* **292**, 95 (1995).

<sup>26</sup>R. H. Liu, J. Yang, M. Z. Pindera, M. Athavale, and P. Grodzinski, *Lab Chip* **2**, 151 (2002).

<sup>27</sup>E. G. Schutt, D. H. Klein, R. M. Mattrey, and J. G. Riess, *Angew. Chem., Int. Ed.* **42**, 3218 (2003).